# ULTRA-FAST WIENER FILTER BASED CRYSTAL IDENTIFICATION ALGORITHM APPLIED TO THE LABPET™ PHOSWICH DETECTORS

H. Camilia Yousefzadeh1, Nicolas Viscogliosi1, Marc-André Tétrault1, Hicham Semmaoui1, Catherine M. Pepin2, Philippe Bérard2, Mélanie Bergeron2, Roger Lecomte2, Réjean Fontaine1

*1 Department of Electrical and Computer Engineering, 2 Department of Nuclear Medicine and Radiobiology, Université de Sherbrooke*

## INTRODUCTION

The LabPET™, a commercial all-digital high resolution small animal APD-based PET scanner [1], [2], uses phoswich detectors to increase pixelization per electronic channel. The novel design of the LabPET™ phoswich detectors consists of two different scintillation crystals, arranged side by side and coupled to an avalanche photodiode (APD) [3].

Various approaches have been proposed to identify the scintillating crystal in phoswich detectors [4]-[9]. The most powerful CI algorithms are digital-based and appear to be derived from the command-and-control theory methods such as the Auto-Regressive Moving-Average with eXogeneous variable (ARMAX) model [10], [11] or on simpler adaptive filter theory approaches relying on Recursive-Least-Square (RLS) or Least-Mean-Square (LMS) algorithms applied to an Auto-Regressive (AR) model [12]. Even though the digital architecture of LabPET™ enables the use of complex CI algorithms, these approaches are computationally expensive and are too time consuming for real-time implementation.

A recent Wiener filter based CI algorithm computes both the crystal light yield ($b_0$) and scintillation decay ($a_1$) constants of each crystal and separate two crystal species by applying a threshold to the $a_1$ spectra [13]. The algorithm was shown to achieve high crystal discrimination accuracy (~98%). The Wiener filter provides an optimum solution and fast calculations for CI, and taking advantage of its highly parallel layout, it can be implemented for real-time computation in high capacity Field Programmable Gate Array (FPGA). However, in its proposed implementation, the non-recursive parameter ($b_0$) was not considered in the CI process, even if it must be computed.

We propose a 2-fold faster implementation of the Wiener filter-based real time CI algorithm, which takes into consideration both the light yield $b_0$ and decay constant $a_1$ parameters of each individual crystal to evaluate the percentage of their contribution in the event signal.

## MATERIALS AND METHODS

In this study, the LabPET™ parallel data acquisition (DAQ) electronic chain was used to collect data. It is a light-to-voltage converter with a shaping stage which consists of an APD, a charge sensitive preamplifier (CSP), an anti-aliasing filter and an analog to digital converter (Fig.1). One phoswich detector module consisting of LYSO-LGSO ($t_r$ ~40 ns and ~65 ns) crystals was investigated in these experiments. Individual crystals of the phoswich had a volume of $2 \times 2 \times$ ~12 mm$^3$ and were placed in optically contact on one long side, and coupled to an APD in a similar fashion as in the LabPET™ modules. The phoswich detector was installed on the DAQ chain and exposed to a 1 mCi $^{68}$Ge rod source of 511 keV annihilation photons. A preprocessing stage consisting of a filtered interpolation, normalization, and decimation was performed before applying the Wiener filter in order to improve the CI performance and to reduce the processing time. The new CI algorithm method consists of two steps: first, a calibration process in which the model of each crystal - in the Z domain - is extracted (Fig. 2.a); second, the DAQ model is incorporated into the crystals model and a Wiener filter evaluates the contribution (in %) of each crystal in the output signal (Fig. 2.b).

### Calibration Process: Crystal Model Extraction

Prior to the fast CI process, a calibration must take place where a model of each individual crystal is empirically estimated through a Wiener filter scheme (Fig. 2). These models take the form of discrete linear, time-invariant (LTI) systems:

$$y(n) = b_0\ x(n) - a_1\, y(n\text{-}1) \qquad (1)$$

where, $b_0$ is the gain coefficient, $a_1$ the crystal decay time and $x(n)$ and $y(n)$, the input data and filter output. Note that $x(n)$ describes the impulse response of the DAQ chain and contains all *a priori* knowledge of the electronic DAQ chain.

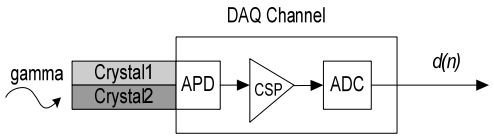


Fig. 1 The LabPET™ data acquisition chain (DAQ). Phoswich detector consisting of two different crystals is excited by a source of 511 keV photons; the recorded signal $d(n)$ is the output signal of the acquisition chain.

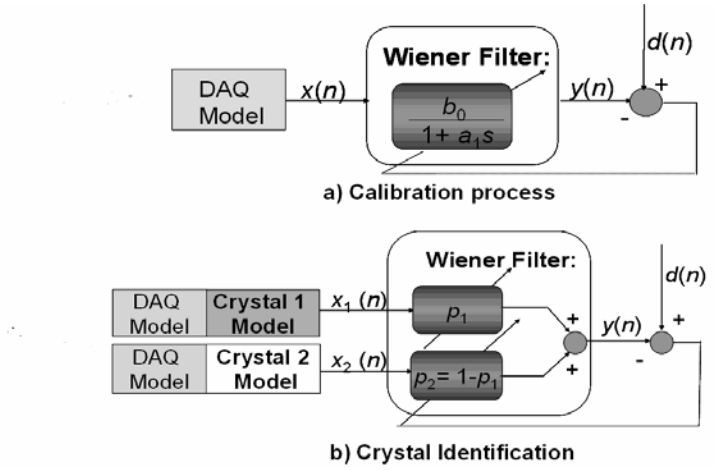


Fig. 2. a) Calibration process based on a Wiener filter algorithm to extract crystal parameters $b_0$ and $a_1$. Recorded events $d(n)$ registered as shown in Fig. 1 are compared to an estimated output signal model for a minimum error. b) The Crystal Identification (CI) process based on a Wiener filter algorithm. The DAQ chain model evaluated in a) is incorporated into the model of each crystal extracted from the calibration process. The individual responses of the DAQ chain and crystals, $x_1(n)$ and $x_2(n)$, are weighted by the contribution (in %) of each crystal, $p_1$ and $p_2$, to generate the output signal.

A specific cost function $J(b_0, a_1)$ minimizes the expected value $E\{\bullet\}$ of the square differences between the recorded event $d(n)$ and the computed output $y(n)$ in order to recover $b_0$ and $a_1$ parameters [13].

The spectra of the $b_0$ and $a_1$ parameters, extracted from a set of 50,000 events acquired at the beginning of the experiment, are spread into two distinct Gaussian-like peaks. After smoothing and fitting both distributions with Gaussian functions, the maximum of each peak is kept and used to generate a model of each crystal [$b_{01}$ $a_{11}$] and [$b_{02}$ $a_{12}$]. The impulse response of each modeled crystal, $h_1(n)$ and $h_2(n)$, at this point will be considered as constant values.

From a signals and systems theory point of view, serially connected LTI sub-systems may be reordered without affecting the behaviour of the higher-level system. Thus, after rearranging the blocks, the digital DAQ model can be incorporated into the model of each crystal to generate the detector impulse responses $x_1(n)$ and $x_2(n)$ (Fig. 2.b). Therefore, $x_1(n)$ and $x_2(n)$ will be incorporated in the next step of the proposed algorithm as *a priori* knowledge.

Ultra-Fast Wiener Filter Based Crystal Identification

Theoretically, the event signal coming from a phoswich detector can be one of these two cases: 1) the signal is issued only from one of the crystals; 2) the signal is colored by both crystals because of Compton scatter within the phoswich detector. Therefore, the output can be considered as the sum of crystals impulse responses weighted by percentages $p_1$ and $p_2$, where $p_1$ and $p_2$ are dependent on the energy deposited in each individual crystal and represent the respective contributions with characteristic frequency signature in the output signal (Fig. 2). As the output signal is normalized, the sum of contributions from crystal 1 and 2 ($p_1$ and $p_2$) can be considered to be equal to one (100%) irrespective of the total energy absorbed in the phoswich detector, including Compton events. Therefore, $p_2$ can be rewritten as 1-$p_1$, and the output signal $y(n)$ will be:

$$y(n) = p_1 x_1(n) + (1 - p_1)\, x_2(n) \qquad (6)$$

As $x_1(n)$ and $x_2(n)$ calculated in the calibration process are invariable impulse responses derived for each individual crystal, the CI process can be reduced to calculate only the percentage contribution of crystal 1 ($p_1$) in the output signal. A threshold applied to $p_1$ will thus identify whether the signal is generated mostly by crystal 1 or crystal 2.

In order to recover $p_1$, a Wiener filter is used to minimize the error between the computed output $y(n)$ and the recorded event $d(n)$ by minimizing a specific cost function $J(p_1)$, the expected value $E\{\bullet\}$ of the square differences between $d(n)$ and $y(n)$.

## RESULTS

Discrimination performances were investigated experimentally. In this study, the crystal 1 is considered as the faster crystal in term of scintillation decay time (LYSO in LYSO-LGSO phoswich) and crystal 2 the slower one (LGSO). Fig. 3 shows the spectra of $a_1$ and $b_0$ extracted from the calibration process for the LYSO-LGSO phoswich detector. The individual crystal models required for the CI step were computed. Figs. 4 shows the spectra of the percentage $p_1$ plotted for the 50,000 events acquired by LYSO-LGSO. A threshold chosen at the optimal minimum of the $p_1$ spectra is then applied for the crystal discrimination. This means that events having a $p_1$ higher than threshold have crystal 1 characteristics while events having $p_1$ smaller than threshold are

assumed to come from crystal 2. As it can be seen in Fig. 5 two Gaussian-like shape peaks appear around 0% and 100% of each $p_1$ spectra, indicating that the majority of events have been absorbed either by crystal 1 ($p_1 \tilde{<} 100$) or by crystal 2 ($p_1 \tilde{<} 0$). Because of an energy resolution of ~ 20% of our system [2], the distributions spread higher than 100% and lower than 0%. Therefore, values in between 0% and 100% are composed from photons that went through a full interaction in one of the two crystals and also from Compton scatters within both crystals.

After applying the identification based on $p_1$ as described above, the $a_1$ spectra were plotted for verification, in order to validate the CI process and calculate the discrimination error. As expected, two clearly separated distributions representing individual crystal events were obtained (Fig. 5). The identification error estimated as the area under the crossing point of the Gaussian curves was < 1.5% for the LYSO-LGSO phoswich detector.

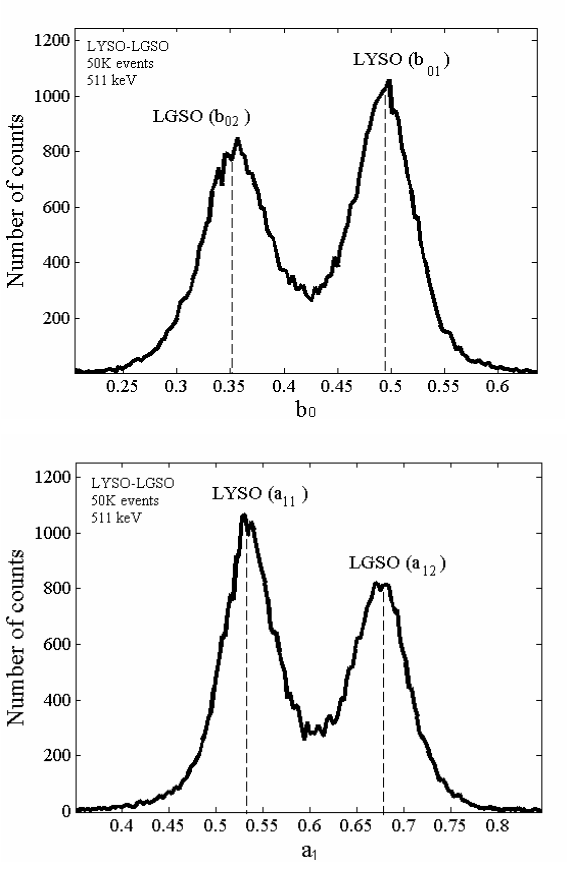


Fig. 3. Spectra of $b_0$ (gain) and $a_1$ (scintillation decay) values obtained for 50,000 events issued from a LYSO-LGSO phoswich detector when exposed to a $^{68}$Ge (511 keV) 1 mCi rod source. Each Gaussian-like distribution peak represents the mean recursive and non-recursive constant values of crystals.

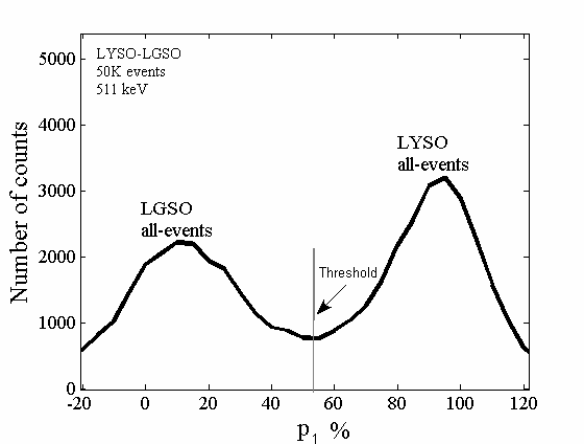


Fig. 4. Spectrum of 50,000 events of p1 (in %) for the LYSO-LGSO phoswich acquired with and without energy thresholding.

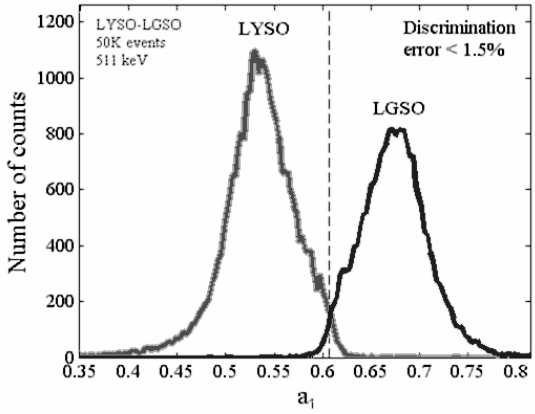


Fig. 5. Crystal identification of LYSO-LGSO phoswich detector shown on $a_1$ spectra

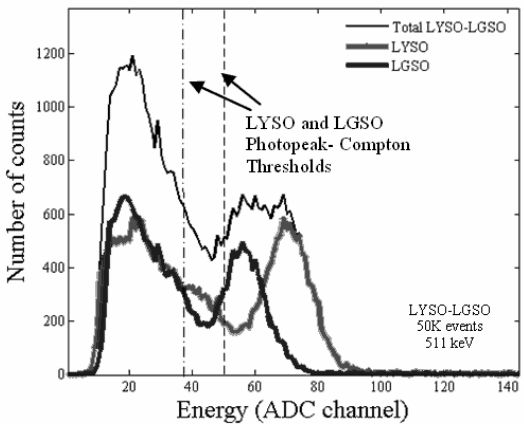


Fig. 6. Energy spectra of LYSO-LGSO phoswich after crystal identification. The lines show the thresholds applied between Compton scatters and photopeak events at crystal granularity.

To further investigate the performance of the algorithm, the energy spectra of detected signals were plotted (Fig. 6). Compton scatter can be thresholded at crystal granularity even for a phoswich detector.

## DISCUSSION AND CONCLUSION

A high-performance real-time CI algorithm was proposed and investigated with a phoswich detector used in the LabPET™. The method achieves at least similar CI rates as other digital methods investigated previously, but at half the computation burden. The proposed method allows the calibration process to be performed for every individual phoswich detector before applying the CI algorithm. Considering the normal variations between detectors in large scale applications like a full-size PET scanner, this is one single major advantage of this method. Moreover, the parallel structure of the Wiener filter algorithm enables high processing speed by taking advantage of the parallel FPGA implementation that is possible with the LabPET™ scanner architecture. The new algorithm takes its major advantage of smaller quantity of identification parameter (%$p_1$) computation and therefore to be at least 2-fold faster than the older Wiener filter algorithm.

Therefore, based on these encouraging results, we foresee that the method could be coupled to a more powerful discrimination algorithm such as ARMAX [10] to discriminate more than two crystals in multi-scintillator detector assemblies for improved granularity or DOI readout.

## REFERENCES


[1] R. Fontaine, F. Bélanger, N. Viscogliosi, H. Semmaoui, M.-A. Tétrault, J.-B. Michaud, C.M. Pepin, J. Cadorette, and R. Lecomte, "The architecture of LabPET™, a small animal APD-based digital PET scanner", *IEEE NSS/MIC Conf. Rec.*, vol. 5, pp. 2785-2789, Puerto Rico, October 2005.

[2] M. Bergeron, J. Cadorette, M. D. Lepage et al., "Performance evaluation of the LabPET™ APD-based digital PET scanner", *2007 IEEE NSS/MIC Conference Record*, (this issue).

[3] A. Saoudi, and R. Lecomte, "A novel APD-based detector module for multi-modality PET/SPECT/CT scanners", *IEEE Trans. Nucl. Sci.*, vol. 46, no. 3, pp. 479-484, June 1999.

[4] R.S. Miyaoka, T.K. Lewellen, H. Yu, and D.L. McDanie1, "Design of a depth of interaction (DOI) PET detector module", *IEEE Trans. Nucl. Sci.*, vol. 45, no. 3, pp. 1069-1073, June 1998.

[5] L.R. Macdonald, M. Dahlbom, "Parallax correction in PET using depth of interaction information", *IEEE Trans. Nucl. Sci.*, vol. 45, no. 4, pp. 2232-2237, August 1998.

[6] V. Astakhov, P. Gumplinger, C. Moisan, T. J. Ruth, and V. Sossi "Effect of Depth of Interaction Decoding on Resolution in PET: A Simulation Study", *IEEE Trans. Nucl. Sci.*, vol. 50, no. 5, pp. 1373-1378, October 2003.

[7] M. Streun, G. Brandenburg, H. Larue, H. Saleh, E. Zimmermann, K. Ziemons, and H. Halling, "Pulse shape discrimination of LSO and LuYAP scintillators for depth of interaction detection in PET", *IEEE Trans. Nucl. Sci.*, vol. 50, no. 3, pp. 344-347, June 2003.

[8] J. S. Huber, W. W. Moses, M. S. Andreaco, and O. Petterson, "An LSO scintillator array for a PET detector module with depth of interaction measurement", *IEEE Trans. Nucl. Sci.*, vol. 48, pp. 684–688, June 2001.

[9] K. C. Burr, A. Ivan, D. E. Castleberry, J. W. LeBlanc, K. S. Shah, and R. Farrell, "Evaluation of a Prototype Small-Animal PET Detector With Depth-of-Interaction Encoding", *IEEE Trans. Nucl. Sci.*, vol. 51, no. 4, pp. 1791-1798, August 2004.

[10] J.-B. Michaud, R. Fontaine, and R. Lecomte, "ARMAX model and recursive least-squares identification for DOI measurement in PET", *2003 IEEE NSS/MIC Conf. Rec.,* vol.4, pp. 2386-2390, 2003.

[11] J.-B. Michaud, R. Fontaine, and R. Lecomte, "Experimental results of identification and vector quantization algorithms for DOI measurement in digital PET scanners with phoswich detectors", *2004 IEEE NSS/MIC Conf. Rec.,* vol.6, pp. 3678-3681, 2004.

[12] H. Semmaoui, N. Viscogliosi, F. Bélanger, J.-B. Michaud, C.M. Pepin, R. Lecomte, and R. Fontaine, "Crystal identification based on recursive-least-squares and least-mean-squares autoregressive models for small animal PET", *IEEE NSS/MIC Conf. Rec.*, vol. 5, pp. 2830-2834, Puerto Rico, October 2005.

[13] N. Viscogliosi, P. Bérard, J. Riendeau, R. Lecomte, R. Fontaine, "Real time implementation of a Wiener filter based crystal identification algorithm for photon counting CT imaging", *IEEE Trans. Nucl. Sci.* (in press).